Cathodoluminescence of zinc and ytterbium oxide poly- and single crystals grown from melt under high pressure

A.N. Baranov,[1,*] M.V. Shestakov,[2] M.V. Chukichev,[3] V.A. Tafeenko,[1] V.A. Mukhanov,[4] V.L. Solozhenko[5]

[1] Chemistry Department, Lomonosov Moscow State University, Moscow, 119991, Russia

[2] Department of Physics, Russian State Agrarian University, Moscow, 127550, Russia

[3] Physics Department, Lomonosov Moscow State University, Moscow, 119991, Russia

[4] Mineral Ltd, Alexandrov, 601650, Russia

[5] LSPM–CNRS, Université Sorbonne Paris Nord, 93430 Villetaneuse, France

ABSTRACT

A mixture of poly- and single crystals of zinc and ytterbium (2 at.%) oxides have been grown from the melt at high temperature (1430°C) and high pressure (3.8 GPa). The crystals were transparent under examination with naked eye. The diameter of crystals was in the range from 0.005 to 2 mm. X-ray diffraction confirmed presence of individual zinc and ytterbium oxides in recovered samples. No change of zinc oxide lattice parameters was revealed comparing to pristine zinc oxide. Cathodoluminescence spectra of the mixture were recorded at 77 and 293 K. The collected spectra exhibit UV, green and near-infrared bands due to exciton recombination, presence of oxygen vacancies and ytterbium ions in ZnO crystals, respectively.

KEYWORDS: single crystal; polycrystal; zinc oxide; ytterbium; cathodoluminescence

[*] Corresponding author: anb@inorg.chem.msu.ru

INTRODUCTION

Zinc oxide is one of the most perspective semiconductors for solar cell up- and downconverters because it's cheap and abundant host for lanthanides [1,2]. The hosted lanthanides can effectively convert UV and visible light into near-infrared range where the c-Si solar cells strongly absorb light [3-6]. The light conversion can occur through non-radiative energy transfer from excited state of ZnO to the excited states of lanthanide ions with subsequent light emission in the infrared range [7-9]. The energy transfer is quite effective process resulting in the efficiency up to 200% when quantum cutting takes place [10].

A number of lanthanides doped ZnO materials, such as composites, films, nanoparticles etc., has already reported in literature [7-9,11-13]. However, it's still unclear whether large number of lantanide ions can be dispersed in ZnO crystalline lattice or the ions can only segregate into crystalline lanthanide oxide due to large charge and radius of trivalent lanthanide ion. Such thermodynamically non-equilibrium method as ion-beam implantation results in incorporation of lanthanide ions in ZnO crystalline lattice with its subsequent out diffusion and segregation upon heat treatment [14,15]. That fact also raises a question whether the luminescent lanthanide centers located in the ZnO or at interface between zinc and lanthanide oxides [7-9].

This work is a follow-up of our previous article on ZnO single crystal growth via spontaneous crystallization from high-temperature melts under high pressure [16]. In that work, the grown ZnO single crystals (up to several millimeters) exhibited strong luminescence in the UV and visible ranges. In the present work, the crystal growth method was adapted for growing a mixture of poly- and single crystals of ZnO and Yb_2O_3, and the recovered samples were studied by scanning electron microscopy (SEM), X-ray diffraction and cathodoluminescence spectroscopy.

EXPERIMENTAL

A mixture of poly- and single crystals of zinc and ytterbium (2 at.%) oxides have been grown from the melt at 3.8 GPa in a toroid-type high-pressure apparatus [16]. The details of the growth method are described elsewhere [17,18]. Microcrystalline powders of ZnO (Alfa Aesar, 99,9995%) and Yb_2O_3 (Alfa Aesar, 99,99%) were thoroughly mixed and grounded in a mortar, then pressed into a pellet and placed into a special gold capsule. The ZnO:Yb_2O_3 molar ratio was equal to 50:1. The samples were gradually compressed up to 3.8 GPa and heated up to 1430^{o}C with an average rate 500^{o}C/min, annealed at this temperature for 2 min and cooled down to 1100^{o}C with an average rate 90^{o}C/min. Crystallization of the melt was observed in the temperature range from 1290 to 1250^{o}C, as evidenced by an increase of electrical resistance of

the high-pressure cell. Finally, the sample was quenched down to room temperature and slowly decompressed. The recovered pellet comprised of a mixture of transparent greenish-yellow crystals with diameters from 0.005 to 0.2 mm.

The morphology and elemental composition of the samples were examined using a LEO Supra 50 VP (Carl Zeiss) high resolution scanning electron microscope equipped with energy dispersive X-ray detector.

The single crystal and powder X-ray diffraction studies were performed using STADIVARI PILATUS100K equipped with a semiconductor detector. The collected patterns were analyzed with WINPLOTR software.

The cathodoluminescence (CL) spectra were measured with a custom-made setup equipped with a pulsed "electron gun" and vacuum cryostat (5×10^{-7} mm Hg). The spectra were recorded using a diffraction grating spectrometer (dispersion 5 Å/mm) and synchronous detector at temperatures of 77 and 300 K. The current and energy were varied within 0.05–2 mA and 10–50 keV ranges, respectively.

RESULTS AND DISCUSSION

A difference of heat dissipation by a top plate and a low piston of hydraulic press results in the temperature gradient in a high-pressure cell of the toroid-type apparatus. The value of the temperature gradient is approximately 10-20^{o}C/mm at 1430^{o}C and 3.8 GPa. That temperature gradient plays a significant role in the process of ZnO crystal growth from the melt. Upon quenching, the crystallization process immediately starts in the top relatively cold part of the cell resulting in a disordered layer of ZnO polycrystals. Further, these polycrystals act as seeds for the crystal growth. Upon further temperature decrease, the ZnO crystals continue to grow along the temperature gradient forming a batch of needle-like crystals.

The crystal growth process changes in the presence of Yb_2O_3 in the initial mixture. Under high pressure and temperature, Yb_2O_3 dissolves in the ZnO melt. Upon quenching Yb_2O_3 crystallizes first forming a layer of polycrystals. The Yb_2O_3 polycrystals act as seeds for subsequent growth of ZnO single crystals.

Fig. 1(a,b) show SEM images of single and multiple ZnO:Yb_2O_3 crystals. One can see large irregular crystals of ZnO with diameters varying from tens of micrometers to 0.1 mm. The small inclusions of Yb_2O_3 crystals are seen on the surface of large ZnO crystals (Fig. 1c). The SEM image of initial Yb_2O_3 crystals is shown in Fig. 1d. They are irregular with diameters much smaller than 1 μm. After crystallization from the melt, Yb_2O_3 crystals become enlarged and grow

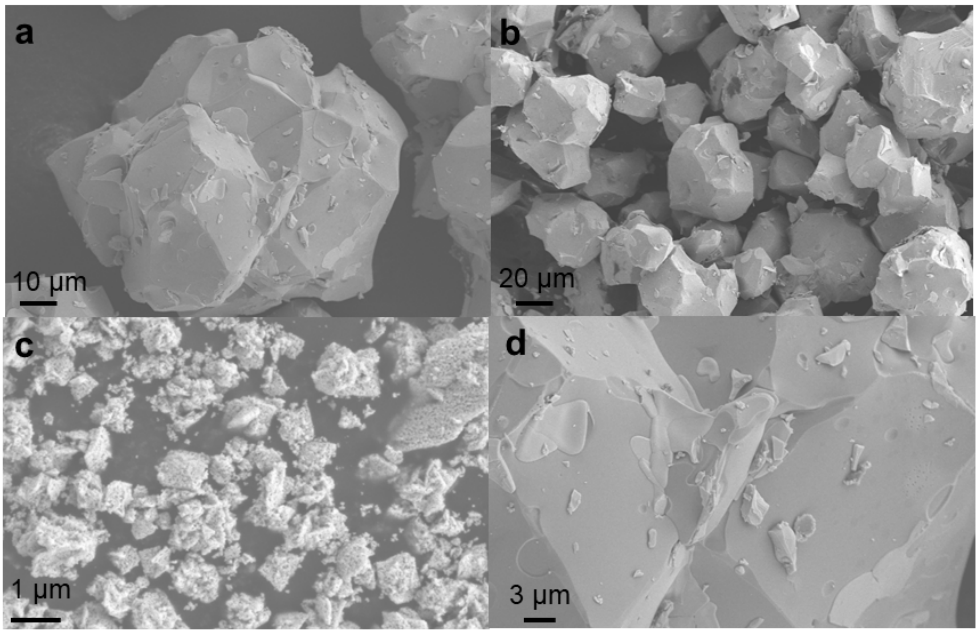

Figure 1 SEM images of ZnO:Yb_2O_3 single crystals (*a*,*b*), and Yb_2O_3 single crystals (initial (*c*) and after crystallization from the melt (*d*)).

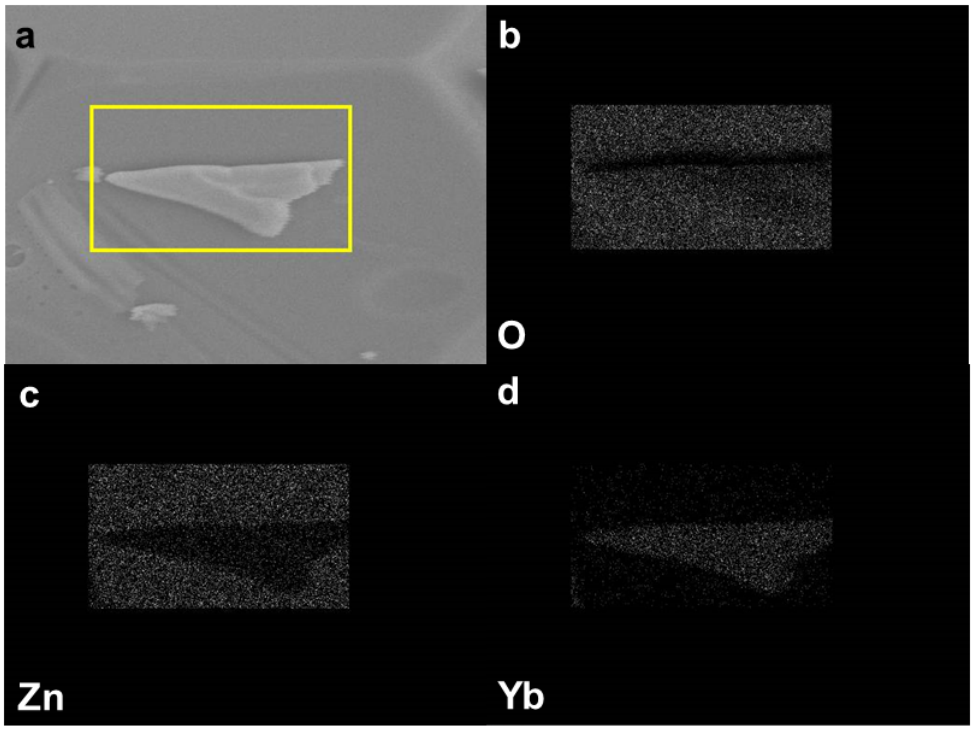

Figure 2 SEM images of ZnO:Yb_2O_3 single crystal (*a*) with the area selected for EDX mapping of oxygen (*b*), zinc (*c*) and ytterbium (*d*).

on the surface of ZnO single crystals. Therefore, the obtained SEM images confirm our hypotheses on the change of crystal growth process after addition of Yb_2O_3 crystals to the melt.

Fig. 2 demonstrates SEM image of ZnO:Yb_2O_3 single crystal area with corresponding elemental maps. The EDX analysis shows that the irregular crystal mostly comprises of Zn and O atoms. The small surface inclusion comprises of Yb and O atoms. Therefore, the EDX analysis supports our hypothesis on very limited (below 0.2%) solubility of Yb_2O_3 in ZnO.

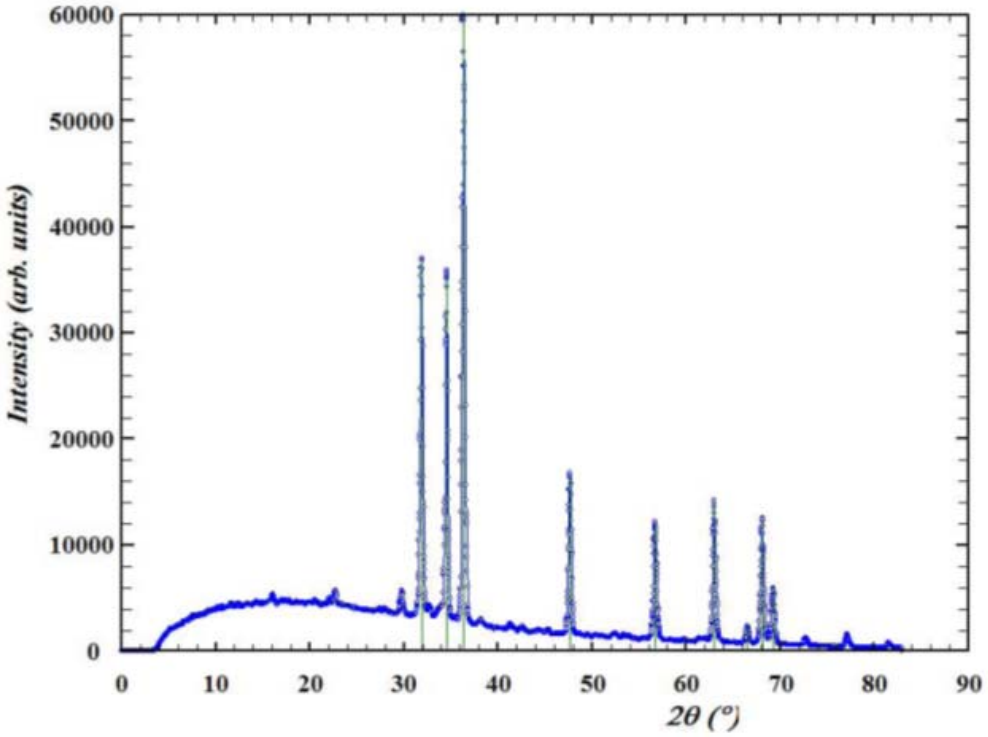

Figure 3 Powder X-ray diffraction pattern of ZnO:Yb_2O_3 crystals

Powder X-ray diffraction pattern of ZnO:Yb_2O_3 crystals is shown in Fig. 3. The pattern contains the reflections corresponding to wurtzite ZnO and cubic Yb_2O_3. The ZnO reflections were indexed with ICDD PDF-2 [36-1451] card and indicated by green bars. The lattice constants of ZnO crystals were determined from powder and single-crystal X-ray diffraction data (Table 1). The obtained values are in good agreement with ICDD PDF-2 [36-1451] card for pure ZnO indicating a low doping level of ZnO by Yb.

Table 1 ZnO unit cell parameters calculated from X-ray diffraction data

X-ray diffraction	*a*=*b*, Å	*c*, Å	V, Å^3
powder	3.248(2)	5.206(2)	47.48
single crystal	3.2503(6)	5.2068(9)	47.64(1)

Fig. 4 shows cathodoluminescence spectrum of undoped ZnO single crystal at room temperature. The excitation of zinc oxide with electrons results in typical UV and green emission bands located in the ranges 350-430 nm and 450-600 nm, respectively. The UV emission is due to radiative recombination of free and bound excitons [19]. The green emission band is associated with various intrinsic defect centers, such as oxygen or zinc vacancies, in ZnO emerging during the synthesis [20].

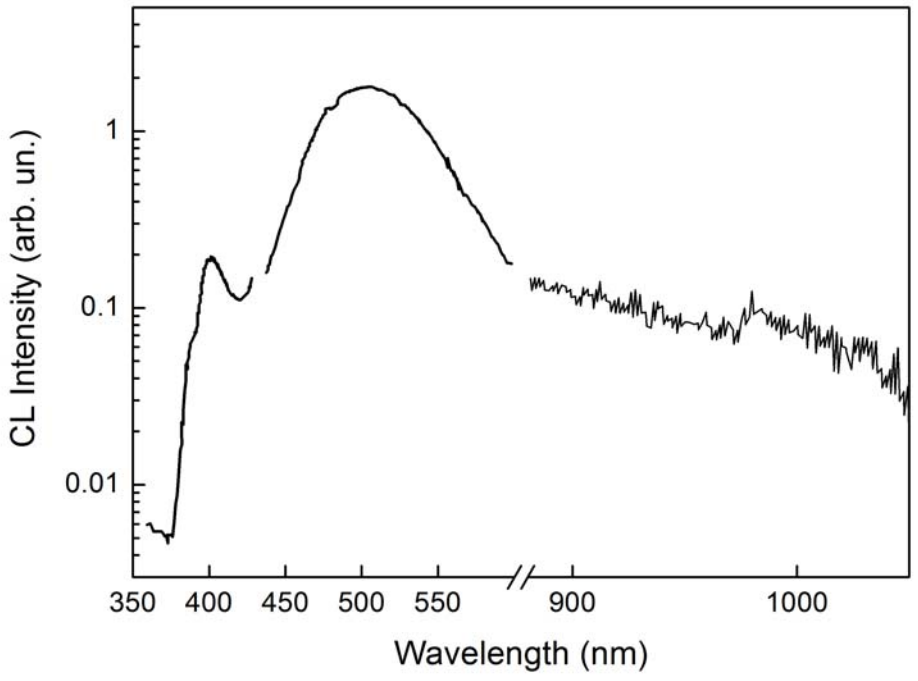

Fig. 4 Cathodoluminescence of undoped ZnO crystal at room temperature

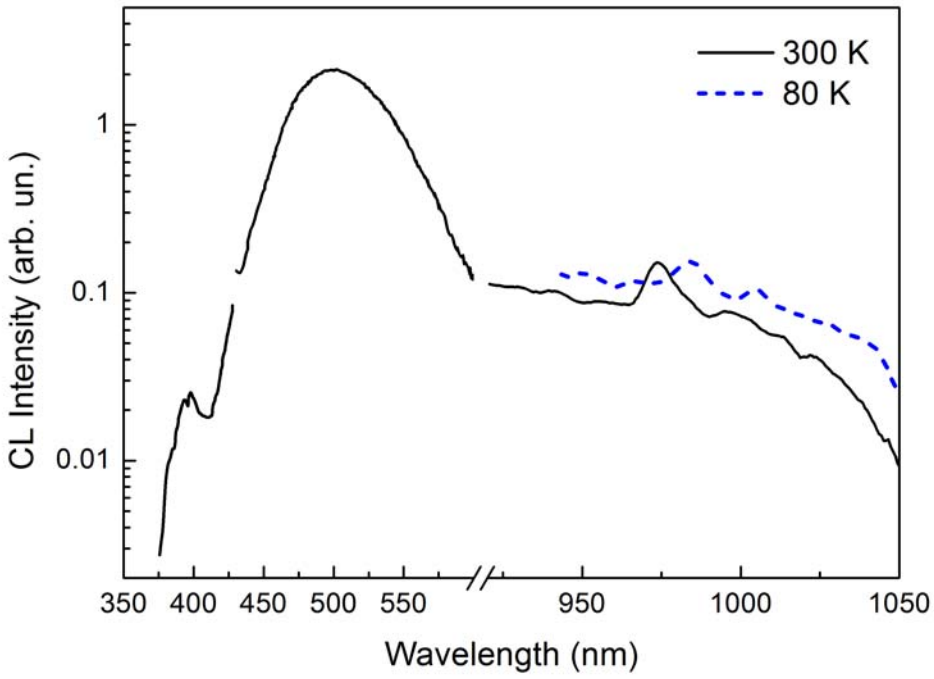

Figure 5 Cathodoluminescence of undoped ZnO:Yb_2O_3 crystal at different temperatures.

Fig. 5 shows cathodoluminescence spectrum of ZnO:Yb_2O_3 single crystals at room and liquid nitrogen temperatures. One can see the UV and visible bands similar to the undoped ZnO, and an infrared band located at 980 nm. Upon addition of Yb_2O_3 to ZnO, the intensity of exciton luminescence decreases while the intensity of green luminescence is virtually unchanged. The infrared band emerges due to radiative electron transition from $^2F_{5/2}$ excited state to $^2F_{7/2}$ ground state in Yb^{3+} ions [7-9]. The intensity of the infrared cathodoluminescence drastically increases upon cooling down the single crystals down to liquid nitrogen temperature. The infrared luminescence band slightly red-shifts, possibly due to the change in electron population of the excited and ground states.

Earlier we reported the synthesis of ZnO/Yb_2O_3 composite for solar spectrum down-conversion [7]. The composite consisted of ZnO nanocrystals with attached tiny Yb_2O_3 nanoparticles. Upon excitation with UV-light, the composite emitted light in the visible and infrared ranges with spectra quite similar to the reported in present paper. The energy transfer from ZnO exciton to Yb^{3+} ions was proposed as possible mechanism of the observed infrared photoluminescence. It's highly likely that similar mechanism of the energy transfer is involved in the infrared cathodoluminescence of ZnO:Yb_2O_3 single crystals. As Yb_2O_3 single crystals are ingrown into

ZnO single crystals, the energy transfer can occur at the interface of two crystal lattices. Further, the ZnO:Yb_2O_3 single crystals may be milled in a planetary mill, encapsulated into a PMMA layer and deposited onto surface of c-Si solar cell for investigation of its efficiency improvement.

CONCLUSIONS

The method of crystal growth from the melt at high pressure was applied for growth of a mixture of poly- and single crystals of zinc and ytterbium oxides. SEM examination revealed that small Yb_2O_3 particles grow on the surface of the resultant ZnO single crystals and act as seeds in the crystallization process. Under electron excitation ZnO:Yb_2O_3 crystals emit light in UV, visible and infrared ranges. The infrared cathodoluminescence (~985 nm) is associated with possible energy transfer from ZnO crystalline host to Yb_2O_3 ingrown particles.

ACKNOWLEDGEMENTS

ANB is grateful to the Université Sorbonne Paris Cité for financial support. The work was supported by the RF President Grant for Leading Scientific Schools (Grant Number 2726.2020.3). The authors acknowledge support from Lomonosov Moscow State University Program of Development for providing access to the XRD and SEM facilities.

CONFLICT OF INTERESTS

The authors declare no conflict of interests.

ORCID IDs

Vladimir L. Solozhenko https://orcid.org/0000-0002-0881-9761

REFERENCES

1. Shohany B.G., Zak A.K., 2020, Ceram. Int., 46, 5507.
2. Marin R., Jaque D., 2021, Chem. Soc. Rev., 121, 1425.
3. Karunakaran S.K., Arumugam G.M., Yang W., Ge S., Khan S.N., Lin X., Yang G., 2021, ACS Sustainable Chem. Eng., 9, 1035−1060.
4. Swart H.C., 2019, Proc. SPIE, 11043, 1104302.
5. Chen D., Wang Y., Hong M., 2012, Nano Energy, 1, 73.
6. Huang X., Han S., Huang W., Liu X., 2013, Chem. Soc. Rev., 42, 173.
7. Shestakov M.V., Baranov A.N., Tikhomirov V.K., Zubavichus Y.V., Kuznetsov A.S., Veligzhanin A. A., Kharin A.Yu., Rösslhuber R., Timoshenko V.Yu., Moshchalkov V.V., 2012, *RSC adv.*, 2, 8783.
8. Shestakov M.V., Tikhomirov V.K., Kirilenko D., Kuznetsov A.S., Chibotaru L.F., Baranov A.N., van Tendeloo G., Moshchalkov V.V., 2011, Optics Express, 19, 15955.
9. Ye S., Jiang N., He F., Liu X., Zhu B., Teng Y., Qiu J.R., 2010, Opt. Express, 18, 639.
10. Rodríguez V.D., Tikhomirov V.K., Méndez-Ramos J., Yanes A.C., Moshchalkov V.V., 2010, Sol. Energy Mater Sol. Cells, 94, 1612.
11. Shalygina O. A., Nazarov I.V., Baranov A.N., Timoshenko V.Yu., 2017, *J. Sol-Gel Sci. Technol.*, 81, 333.
12. Kalaiezhily R. K., Asvini V., Saravanan G., Ravichandran K., 2019, Dalton Trans., 48, 12228.
13. Heng C.L., Wang T., Su W.Y., Wu H.C., Yang M.C., Deng L.G., Yin P.G., Finstad T.G., 2017, J. Alloys Compd., 695, 2232.
14. Nekvindová P., Cajzl J., Macková A., Malinský P., Oswald J., Böttger R., Yatskiv R., 2020, J. Alloys Compd., 816, 152455.
15. Miranda S., Peres M., Monteiro T., Alves E., Sun H., Geruschke T., Vianden R., Loren K., 2011, Opt. Mater., 33, 1139.
16. Mukhanov V.A., Sokolov P.S., Baranov A.N., Timoshenko V.Yu., Zhigunov D.M., Solozhenko V.L., 2013, *CrystEngComm*, 15, 6318.
17. Baranov A.N., Sokolov P.S., Kurakevych O.O., Tafeenko V.A., Trots D., Solozhenko V.L., 2008, High Pressure Res., 28, 515,
18. Mukhanov V. A., Sokolov P. S., Solozhenko V. L., 2012, J. Superhard Mater., 34, 211
19. Witkowski B.S., Wachnicki L., Gieraltowska S., Reszka A., Kowalski, B.J., Godlewski M., 2015, Microsc. Microanal., 21, 564.
20. Nagase T., Kominami H., Nakanishi Y., Shinozaki K., Mizutani N., 2010, Thin Solid Films, 518, 3875.